Analytical and Bioanalytical Chemistry (2022) 414:1623–1630
https://doi.org/10.1007/s00216-021-03784-9

RESEARCH PAPER

One-step hydrothermal synthesis of WS_2 quantum dots as fluorescent sensor for sensitive and selective recognition of hemoglobin and cardiac biomarker myoglobin

Tianqun Song[1] · Qinglian Wang[1] · Hongxia Yu[1] · Wanting Gao[1] · Yixin Xu[1] · Yixin Lv[1] · Yanzhi Xing[1] · Yifeng Chen[1] · Mei Yang[1]

Received: 8 September 2021 / Revised: 24 October 2021 / Accepted: 9 November 2021 / Published online: 7 January 2022

Abstract

Transition metal dichalcogenide (TMD) dots exhibit excellent photoluminescence performance due to the quantum confinement effect and edge effect, and are extensively applied in electronic and optical devices, sensors, catalysis, and bioimaging. In this work, WS_2 quantum dots (WS_2 QDs) were prepared under a simple one-step hydrothermal method by optimizing the reaction conditions, and a quantum yield of 11.23% was achieved. The as-prepared WS_2 QDs possess good photo-bleaching resistance, salt tolerance, and pH stability. The fluorescence investigations showed that the WS_2 QDs acted as a highly efficient fluorescent sensor to detect hemoglobin (Hb) and cardiac biomarker myoglobin (Myo). The linear range was 1–600 μg/mL for Hb and 0.01–120 μg/mL for Myo, with detection limits as low as 260 and 7.6 ng/mL, respectively. Importantly, the WS_2 QDs were used to determine the Hb/Myo content in human blood/serum samples, with satisfactory results, indicating that this technique holds promise for application in clinical diagnosis associated with Hb/Myo levels. To the best of our knowledge, this is the first example of TMD QDs without any modification as a fluorescent sensor for detecting Hb and Myo simultaneously.

Keywords Transition metal dichalcogenides (TMDs) · Quantum dots (QDs) · Fluorescent sensor · Hemoglobin · Myoglobin

Introduction

Hemoglobin (Hb) and myoglobin (Myo) are heme-containing proteins, which play important roles in many biological functions of living organisms. Hb is present in red blood cells and is mainly responsible for transporting O_2 and CO_2 between the respiratory system and other organs. Abnormal levels of Hb in the body are related to diseases such as anemia, hematuria, leukemia, and sickle cell disease [1, 2]. The main function of Myo in the body is to transport and store O_2 for muscle tissue by reversibly combining and releasing O_2. Myo is an important biomarker of early acute myocardial infarction (AMI) [3]. When the myocardium or skeletal muscle is damaged, Myo, as a small molecule of globulin released from the muscle tissue, will penetrate the circulating blood, leading to high blood Myo levels [4]. Therefore, the determination of Hb and Myo is of great importance in the diagnosis of diseases. Due to the low concentration of Myo in serum (6–100 ng/mL) [3], the detection method should have high sensitivity and a low detection limit; otherwise, the blood sample needs to be enriched and concentrated before detection, which is very time-consuming and complicated. To date, various methods for detecting Hb and Myo have been developed, including electrochemistry [5, 6], absorption spectrometry [7], fluorimetry [8, 9], surface plasmon resonance (SPR) sensing [10], immunoassay [11], and high-performance liquid chromatography [12]. In contrast to these methods, fluorescence (FL) detection is inexpensive, rapid and simple, sensitive, and selective, and may be able to meet the requirements. However, some fluorescent sensors of Hb and Myo such as certain metal complexes and dyes have low sensitivity [13], which limits their application. Therefore, the preparation of highly efficient fluorescent sensor materials has become a huge challenge.

✉ Mei Yang
yangmeils@163.com

[1] School of Chemistry and Chemical Engineering, Liaoning Normal University, Dalian 116029, China

Transition metal dichalcogenides (TMDs) are a class of semiconductor materials with a graphene-like structure. Bulk TMDs have a hexagonal layered structure, and the layer is a S-M-S sandwich structure in which chalcogen atoms and metal atoms are bonded by strong covalent bonds [14]. The layers are bound together by weak van der Waals forces. Compared with the zero band gap of graphene, the change from indirect to direct band gap caused by the exfoliation of TMDs from bulk to layered form makes it suitable for applications including semiconductor-based electronic and optical devices [15, 16], sensors [17–19], catalysis [20, 21], and bioimaging [22, 23]. Similar to graphene, when the size of TMDs is less than 10 nm, TMD quantum dots (TMD QDs) are obtained. Owing to the quantum confinement effect and edge effect, the photoluminescence performance of TMD QDs is significantly enhanced [24]. In TMDs, molybdenum disulfide (MoS_2) is the most widely studied material, and some progress has been made, but research on other TMD QDs such as tungsten disulfide (WS_2), molybdenum diselenide ($MoSe_2$), and tungsten diselenide (WSe_2) QDs is still in its infancy, and is thus still challenging. Compared with MoS_2 QDs, WS_2 QDs also exhibit strong photoluminescence properties, simple preparation, excellent water solubility and biocompatibility, and low toxicity, thus making them attractive candidates for use as biosensors [25].

In this contribution, WS_2 QDs were prepared via a simple one-step hydrothermal method using $Na_2WO_4{\cdot}2H_2O$ and glutathione (GSH), with a quantum yield (QY) of 11.23%. In addition, the WS_2 QDs were found to possess good photobleaching resistance, salt tolerance, and pH stability. The FL investigations showed that WS_2 QDs can act as a highly sensitive and selective fluorescent sensor to detect Hb and cardiac biomarker Myo, with detection limits as low as 260 and 7.6 ng/mL, respectively. Importantly, WS_2 QDs were used to determine Hb/Myo content in human blood/serum samples, with satisfactory results, and thus hold promise for application in diagnostic and biochemical analysis of Hb and Myo.

Experimental

Chemicals and materials

Sodium tungstate ($Na_2WO_4{\cdot}2H_2O$), L-cysteine (L-Cys), potassium dihydrogen phosphate (KH_2PO_4), and dipotassium phosphate ($Na_2HPO_4{\cdot}12H_2O$) were purchased from Tianjin Komiou Reagent Company. Glutathione (GSH) was obtained from Dalian Meilun Biotechnology Co., Ltd. Quinine sulfate ($C_{40}H_{48}N_4O_4{\bullet}H_2SO_4$ QS) was obtained from Shanghai Yuanye Biological Technology Co., Ltd. Red blood cell lysis solution was obtained from Nanjing SenBeiJia Biological Technology Co., Ltd. Dialysis bags (MW 3500 Da, flat width 44 mm) were purchased from Beijing Solarbio Science & Technology Co., Ltd. The experimental reagents were all of analytical grade, and the water used was double-distilled water.

Apparatus

Transmission electron microscopy (TEM) and atomic force microscopy (AFM) images were collected with JEOL JEM-2000EX (Japan) and OXFORD TS-150 instruments (USA), respectively. X-ray photoelectron spectroscopy (XPS) was conducted using an ESCALAB 250Xi instrument (Al-Kα, USA). Infrared (IR) spectra were measured on a Bruker TENSOR II spectrometer (KBr pellet, Germany). UV-Vis spectra were obtained on a Hitachi U-3900 spectrophotometer (Japan). FL lifetime was determined using a HORIBA FluoroMax-4-TCSPC [time-correlated single-photon counting] (USA). The FL spectra were recorded on a Hitachi F-7000 fluorescence spectrometer (Japan).

Preparation of WS_2 QDs

WS_2 QDs were prepared using different raw materials under hydrothermal conditions, with some modifications compared to the reported method [26].

Method 1: Firstly, $Na_2WO_4{\cdot}2H_2O$ (0.15 g) was dissolved in 7.5 mL water, and GSH (0.56 g) was dissolved in 10 mL water. The two solutions were then mixed well. The mixture was transferred to a 50-mL Teflon autoclave, heated at 200 °C for 8 h, and then cooled at 30 °C. The obtained yellow clear solution was dialyzed in water. After drying at 50 °C, powder of dark yellow WS_2 QDs was collected, then dispersed in water, stored at 4 °C, and ultrasonicated before use. In order to optimize the dosage and reaction time, only the mass of GSH and the heating time were adjusted, and other conditions were unchanged.

Method 2: Firstly, $Na_2WO_4{\cdot}2H_2O$ (0.15 g) was dissolved in 15 mL water, and L-Cys (0.22 g) was dissolved in 10 mL water. The two solutions were then mixed well. The mixture was transferred to a 50-mL Teflon autoclave, heated at 200 °C for 8 h, and then cooled at 30 °C. The product was centrifuged at 8000 rpm for 40 min. The pale yellow supernatant was collected and dialyzed in water. After drying at 50 °C, powder of pale yellow WS_2 QDs was collected, then dispersed in water, stored at 4 °C, and ultrasonicated before use. In order to optimize the dosage and reaction time, only the mass of L-Cys and the heating time were adjusted, and other conditions were unchanged.

Fluorescence measurement

The process for using WS_2 QDs as a fluorescent sensor to detect Hb and Myo is as follows. WS_2 QDs and different concentrations of Hb/Myo were diluted to 2 mL with pH 7.5 phosphate-buffered saline (PBS) solution. The final concentration of WS_2 QDs was 0.08/0.05 mg mL^{-1}. The FL spectra were obtained on a Hitachi F-7000 fluorescence spectrometer at $\lambda_{ex} = 317$ nm. The FL intensity of the WS_2 QDs with and without the addition of Hb/Myo was indicated as F and F_0, respectively.

Pretreatment of human blood samples

Human blood samples from healthy volunteers in our lab (obtained by Liaoning Normal University School Hospital) were collected in anticoagulation tubes and centrifuged at 2000 rpm for 15 min. The upper layer of the serum, used for the measurement of Myo, was diluted 10 times with PBS 7.5 before use. Hb is mainly present in the mature red blood cells of the lower layer. Red blood cell lysis solution was added to the red blood cells (volume ratio 1:1) and then packed into 1.5-mL centrifuge tubes. After oscillation for 30 min, the centrifuge tubes were stored overnight at 4 °C, and then centrifuged at 8000 rpm for 30 min. The supernatant was used to determine the Hb in the sample, and was diluted 2000-fold with PBS 7.5 to reduce interference before the test.

Results and discussion

Preparation and characterization of WS_2 QDs

WS_2 QDs were synthesized using a one-step hydrothermal method by optimizing the type of sulfur source, dosage, and reaction time. When $Na_2WO_4{\cdot}2H_2O$ and L-Cys with different molar ratios were used as reactants, WS_2 QDs were obtained by reacting for 8 h at 200 °C. The results showed that when the tungsten-to-sulfur molar ratio was 1:4, the QY of the obtained WS_2 QDs was the highest, at 7.70% (Table S1 entry 2). Therefore, a tungsten-to-sulfur ratio of 1:4 was used with reaction times of 4, 8, 12, and 24 h, and the QY of the obtained products was measured (Table S1 entries 2 and 4–6). The results revealed that the highest QY was achieved with a reaction time of 8 h. It was also found that the reaction temperature had almost no effect on the QY of the WS_2 QDs. Therefore, $Na_2WO_4{\cdot}2H_2O$ and L-Cys with a tungsten-to-sulfur molar ratio of 1:4 were chosen to react at 200 °C for 8 h.

In order to explore whether changing the type of sulfur source could improve the QY of the WS_2 QDs, L-Cys was replaced with GSH, and the reaction was carried out at 200 °C for 8 h. It was found that the highest QY (11.23%) was achieved at a tungsten-to-sulfur molar ratio of 1:4, and was higher than the result with L-Cys as the sulfur source (Table S2 entry 3). The reaction was also carried out at other reaction times under the same temperature. As shown in Table S2 entries 6–8, the WS_2 QDs synthesized with GSH as the sulfur source had higher QY than those with L-Cys as the sulfur source. It was speculated that this was because the chemical bonds in the GSH peptide chain composed of glutamic acid, cysteine, and glycine were broken during the hydrothermal condition, and amino acid residues occupied the surface defects of the WS_2 QDs, which improved the QY of the WS_2 QDs. Therefore, in subsequent experiments, using $Na_2WO_4{\cdot}2H_2O$ and GSH with a molar ratio of tungsten to sulfur of 1:4, WS_2 QDs were prepared at 200 °C for 8 h, with QY of 11.23% and FL lifetime of 3.08 ns. Table 1 lists the fluorescence QY of WS_2 QDs synthesized by hydrothermal methods reported in the literature, indicating that WS_2 QDs prepared under a relatively short time in this work had good FL properties.

The obtained WS_2 QDs were characterized by TEM, AFM, XPS, and FT-IR. The size distribution of the WS_2 QDs was recorded by TEM. It can be seen from Fig. 1a that WS_2 QDs had good monodispersity and relatively uniform size distribution from 1.6 to 2.3 nm, and the average particle size was 1.9 nm (Fig. 1a inset). AFM images were recorded to confirm the thickness of the WS_2 QDs (Fig. 1b). The results showed that the thickness of the WS_2 QDs was about 0.95 nm, which was consistent with the thickness of monatomic-layer WS_2 QDs of 0.8–1.0 nm reported in the literature [27], proving that the synthesized WS_2 QDs comprised a monatomic layer with good dispersion. Using EDS to analyze the WS_2 QDs, it was clearly seen that the WS_2 QDs contained the five elements of W, S, C, N, and O, which proved that W and S were present in the synthesized QDs, and C, N, and O were the surface functional groups of the WS_2 QDs (Fig. S1).

XPS analysis was performed to further verify the surface composition and the chemical states of the WS_2 QDs. The

Table 1 The fluorescence QY of WS_2 QDs obtained by hydrothermal methods reported in the literature

QDs	Raw materials	t (h)	T (°C)	QY (%)	Ref.
WS_2	WS_2 nanosheets	6	200	1.8	[27]
WS_2	Na_2WO_4, L-Cys	24	180	3.05	[28]
f-WS_2	Na_2WO_4, L-Cys	36	200	4.04	[17]
WS_2	WS_2 powder	24	220	4.9	[29]
2H-WS_2	1 T-WS_2 nanosheets	1.5	100	5.5	[30]
WS_2	Na_2WO_4, GSH	24	220	6.6	[26]
WS_2	Na_2WO_4, L-Cys	24	220	10.1	[31]
WS_2	Na_2WO_4, GSH	8	200	11.23	This work

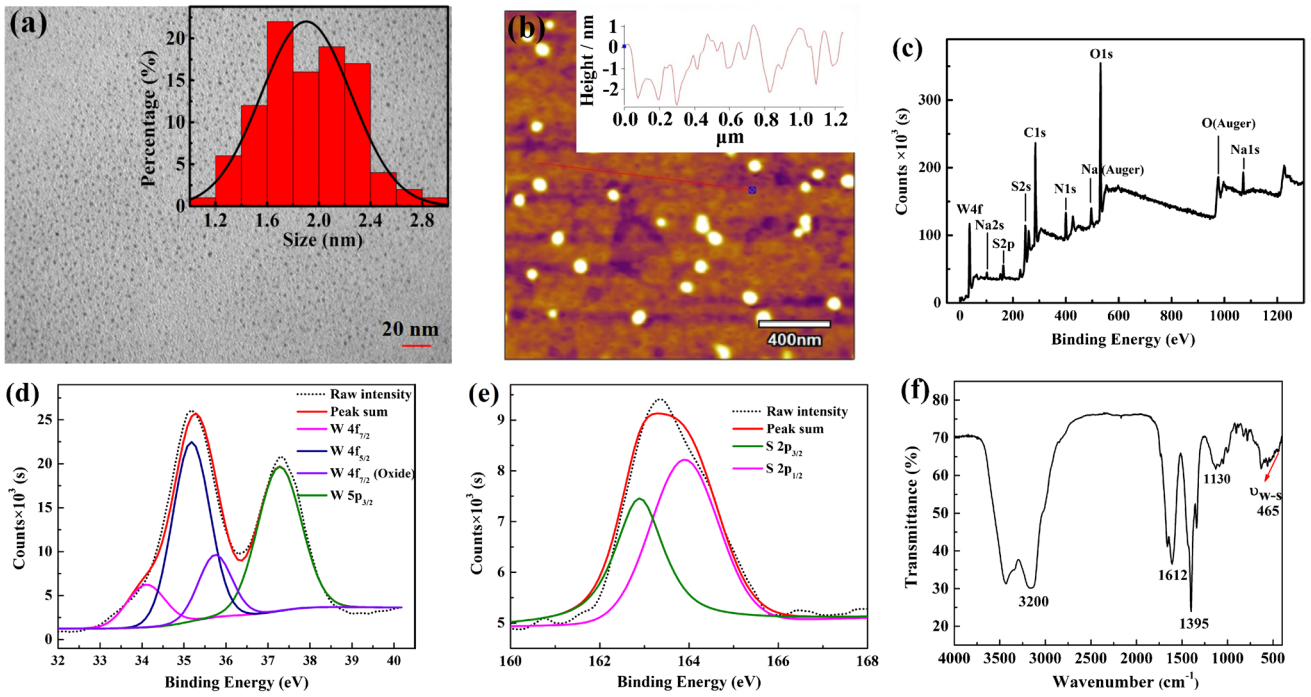

Fig. 1 **a** TEM image of WS_2 QDs. Inset: the particle size distribution histogram of WS_2 QDs. **b** AFM image of WS_2 QDs. **c** The survey scan XPS spectrum of WS_2 QDs. High-resolution peak-fitting XPS spectra of **d** W 4*f* region and **e** S 2*p* from WS_2 QDs. **f** FTIR spectrum of WS_2 QDs

whole spectrum showed the elemental peaks of W and S, as well as C, N, O, and Na, from the reactants of hydrothermal conditions (Fig. 1c) [26]. The $4f_{7/2}$, $4f_{5/2}$, and $5p_{3/2}$ peaks of W in WS_2 QDs appeared at 34.1, 35.1, and 37.2 eV, respectively, which indicated the existence of W^{4+} (Fig. 1d). Besides, the peak around 35.7 eV was attributed to the binding energy of W^{6+}, being from the oxidation state of W [28, 29]. As shown in Fig. 1e, the peaks near 163.9 and 162.9 eV corresponded to the concomitant S $2p_{1/2}$ and $2p_{3/2}$, respectively, which originated from the oxidation state of S^{2-} [27].

Additionally, the synthesized WS_2 QDs were further verified by IR. As shown in Fig. 1f, the peaks at 3200 and 1395 cm^{-1} were the stretching vibration peak and the in-plane stretching vibration peak of N–H from $–NH_2$, respectively. The peak at 1612 cm^{-1} was assigned to the stretching vibration of the C=O bond, indicating the existence of –COOH. As the WS_2 QDs contained $–NH_2$ and –COOH groups, it had good water solubility. In addition, the weak peak at 465 cm^{-1} was ascribed to the characteristic peak of W–S, and the characteristic peak of the S–H stretching band at 2524 cm^{-1} disappeared [26], all of which indicated that the WS_2 QDs had been successfully synthesized.

Optical studies

To explore the optical performance of the WS_2 QDs, UV-Vis and FL spectra were used to characterize the WS_2 QDs. As shown in Fig. S2, a weak absorption peak appeared near 270 nm, characteristic of the excitonic feature of the WS_2 QDs [27]. Figure 2a shows the FL spectra of the WS_2 QDs with excitation wavelength from 270 to 400 nm. The position of the maximum emission peak was redshifted, and the peak intensity gradually increased and then decreased, reaching a maximum value of 425 nm with an excitation wavelength of 320 nm, indicating that the synthesized WS_2 had excitation wavelength dependence. The surface defects and the polydispersity of QDs may cause a size-dependent effect, leading to the possibility of excitation wavelength dependence of QDs [32]. As shown in Fig. 2b, the FL spectra of the WS_2 QDs indicate a maximum excitation and emission wavelength of 317 and 425 nm, respectively. The WS_2 QDs showed good photoluminescence properties due to the edge effect and quantum confinement effect of the TMD zero-dimensional materials [24].

In order to apply the WS_2 QDs in practice, different illumination times, salt concentrations, and pH values were investigated to evaluate the photoluminescence stability of the WS_2 QDs. The photo-bleaching resistance of QDs is an important indicator for evaluating fluorescent reagents. In the experiment, the WS_2 QDs were continuously irradiated under 317-nm excitation light for 1 h, and the results revealed that the FL intensity of the WS_2 QDs hardly changed, indicating that the WS_2 QDs had

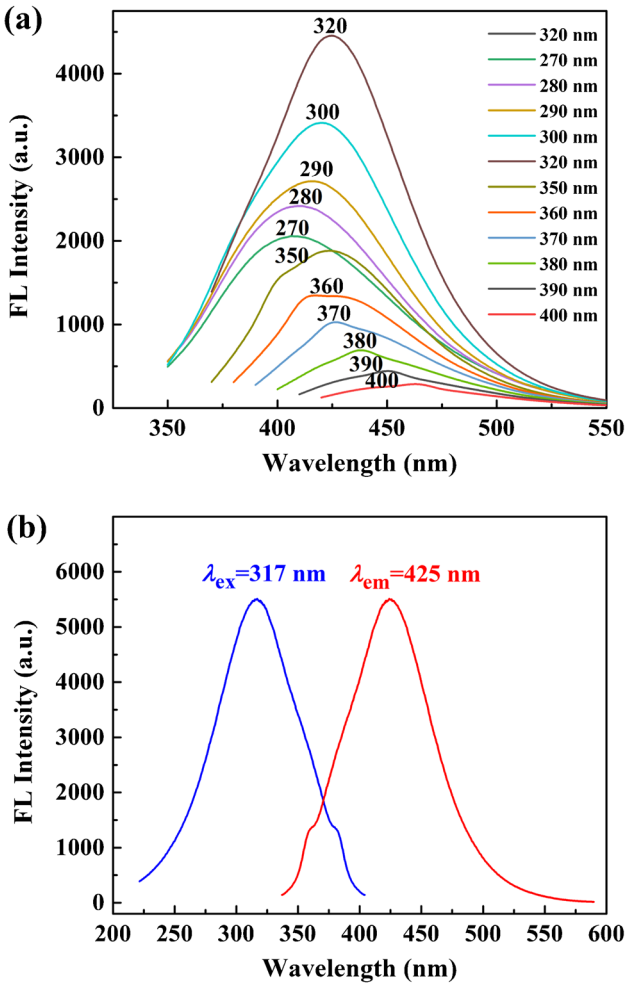

Fig. 2 **a** FL spectra of WS_2 QDs excited by various wavelengths ($c_{WS2\ QDs}$ = 0.04 mg/mL). **b** FL spectra of WS_2 QDs ($c_{WS2\ QDs}$ = 0.05 mg/mL)

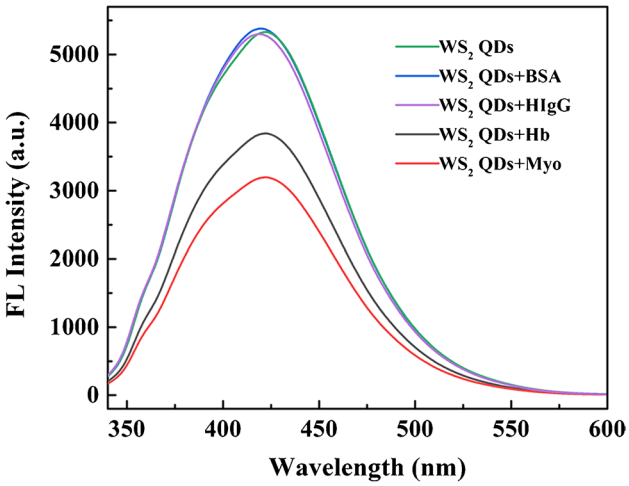

Fig. 3 The FL spectra of WS_2 QDs in 200 μg/mL of different proteins (λ_{ex} = 317 nm)

good light stability and strong photo-bleaching resistance (Fig. S3). These properties make it possible for the WS_2 QDs to be used as fluorescent probes in the fields of biosensing and cell imaging. The electrolyte in the organism is mainly NaCl. The presence of salt may cause the aggregation of WS_2 QDs and change the FL properties. Therefore, the salt tolerance of the WS_2 QDs was studied. As shown in Fig. S4, in the presence of high concentrations of NaCl, the FL intensity of the WS_2 QDs was basically unchanged, indicating that the WS_2 QDs had good salt resistance, which provides advantages for their application in real biological sample analysis. In addition, the FL intensity of the WS_2 QDs was tested under different pH PBS buffer solutions (Fig. S5). The results showed that the FL intensity of the WS_2 QDs was stable at pH 5.0–9.0. In summary, the synthesized WS_2 QDs had good photobleaching resistance, salt tolerance, and pH stability.

Fluorescence detection of Hb and Myo

Proteins play an important role in the human body, so it is necessary to test whether WS_2 QDs can be used as a fluorescent sensor for proteins. Figure 3 shows the FL intensity when human immunoglobulin G (HIgG), bovine serum albumin (BSA), Hb, and Myo were added to the WS_2 QDs. Only Hb and Myo were found to have a significant quenching effect on the WS_2 QDs, suggesting that the WS_2 QDs could selectively detect Hb and Myo. The UV-Vis absorption peaks of Hb and Myo were observed at 409 nm, which overlapped with the emission of the WS_2 QDs (Fig. S6). Therefore, the fluorescence resonance energy transfer (FRET) process occurred from the WS_2 QDs to Hb/Myo, resulting in FL quenching of the WS_2 QDs.

To achieve optimal detection performance, the concentration of WS_2 QDs, pH, and reaction time were optimized. When the concentration of WS_2 QDs was 0.08 and 0.05 mg/mL, Hb and Myo could quench the FL intensity of the WS_2 QDs to the greatest extent, respectively (Fig. S7). Under the condition of PBS 7.5, the quenching degree of the WS_2 QDs reached the maximum with the existence of Hb or Myo (Fig. S8). Finally, the sample was incubated for 60 min, and the FL value was recorded every 10 min. The results are shown in Fig. S9, indicating that the incubation time had almost no effect on the quenching degree of WS_2 QDs by Hb/Myo. Therefore, 0.08 and 0.05 mg/mL WS_2 QDs were used in the subsequent experiments to detect Hb/Myo under the condition of PBS 7.5.

To investigate the performance of the WS_2 QDs for detecting Hb/Myo, Hb/Myo with different concentrations was added to WS_2 QD solution. The final concentration range of Hb and Myo was 0–1200 μg/mL and 0–300 μg/mL, respectively. As shown in Fig. 4, the FL intensity of the

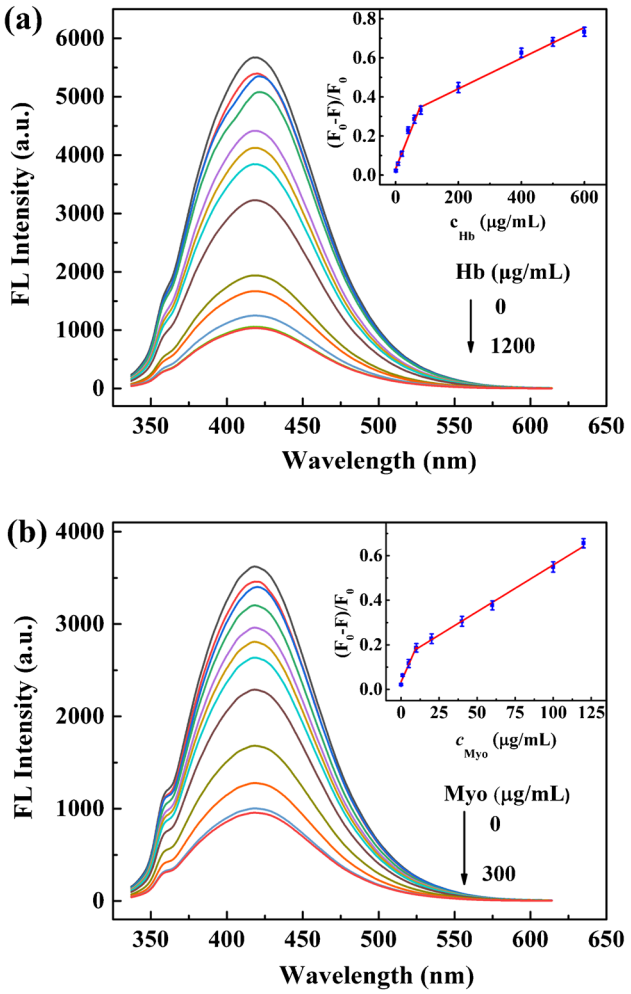

Fig. 4 FL spectra of WS_2 QDs with different concentrations of Hb (**a**) and Myo (**b**); the inset: the linear relationship between $(F_0 - F)/F_0$ and Hb/Myo concentration

WS_2 QDs gradually decreased as the Hb/Myo concentration increased. To further investigate the relationship between the quenching effect and Hb/Myo concentration, plots of FL intensity versus Hb/Myo concentration were obtained. It was seen that the Hb/Myo concentration obeyed two linear relationships with $(F_0 - F)/F_0$. The linear equations were $(F_0 - F)/F_0 = 4.1 \times 10^{-3} c_{Hb}$ (μg/mL) + 0.031 (R = 0.993) and $(F_0 - F)/F_0 = 7.8 \times 10^{-4} c_{Hb}$ (μg/mL) + 0.29 (R = 0.993) with concentration ranges of 1–80 μg/mL and 80–600 μg/mL, respectively. For Myo, the linear equations were $(F_0 - F)/F_0 = 1.6 \times 10^{-2} c_{Myo}$ (μg/mL) + 0.034 (R = 0.987) and $(F_0 - F)/F_0 = 4.2 \times 10^{-3} c_{Myo}$ (μg/mL) + 0.14 (R = 0.998) with concentration ranges of 0.01–10 μg/mL and 10–120 μg/mL, respectively. The break of curves may be due to the fact that WS_2 QDs agglomerate with the addition of a high concentration of protein, which could be seen from the TEM images (Fig. S10). The aggregation of the WS_2 QDs led to a slower drop in FL intensity. Therefore, the slope became smaller at high concentrations, which was consistent with the conclusions in the reported literature [33, 34]. As a whole, WS_2 QDs could quantitatively detect Hb/Myo concentrations in the range of 1–600 μg/mL/0.01–120 μg/mL. If the concentration of Hb/Myo falls in the content range near the break, the quantitative result may be inaccurate. The sample should be diluted to adapt to the linear range of low concentrations to overcome such inaccuracy. In addition, a calibration curve directly using serum samples to detect Myo was developed (Fig. S11). It was observed that the quenching rate constant (slope in the linear equations) was quite different only at low concentrations with and without serum sample, indicating that serum samples would interfere with the detection of Myo at low concentrations. Due to the low concentration of Myo in serum, a real serum sample was diluted 10 times so that it hardly interfered with Myo detection.

The FL intensity of the WS_2 QDs with Hb/Myo was measured in parallel 11 times to calculate the relative standard deviations (RSD) for evaluating the precision of this method, and the results were 2.2% (5 μg/mL) and 2.1% (100 μg/mL) for Hb, and 1.9% (0.05 μg/mL) and 1.5% (10 μg/mL) for Myo, which showed good precision for detecting Hb/Myo. The detection limit of Hb and Myo was calculated to be 260 and 7.6 ng/mL (S/N = 3), respectively. Compared with the reported literature (Tables S3, S4), our method for detecting Hb/Myo has a wide linear range and low detection limit, and can act as a highly efficient fluorescent sensor.

Selectivity of WS_2 QD sensor

Due to the complexity of real sample composition, coexisting components may affect the determination of Hb/Myo. Therefore, we investigated the interference of common ions and coexisting components on the system. When the concentration of Hb/Myo was 10/0.1 μg/mL, the FL quenching

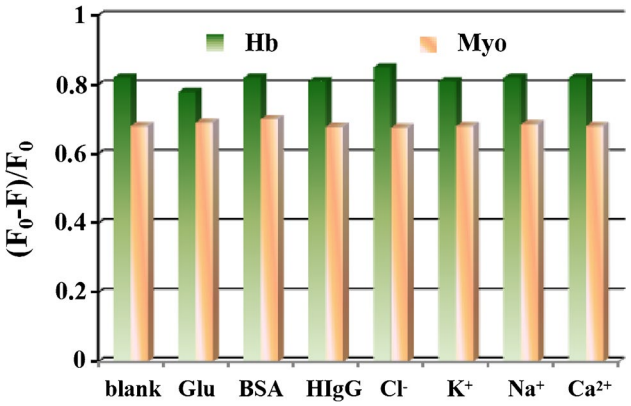

Fig. 5 $(F_0 - F)/F_0$ value of WS_2 QDs and the Hb/Myo system without (blank) and with the presence of Glu, BSA, HIgG, Cl^-, K^+, Na^+, and Ca^{2+} (λ_{em} = 425 nm). The concentration of the interfering agent was 1000 times that of Hb/Myo

Table 2 Detection results for Hb in human blood samples [a]

Samples	Measured value (mg/mL)	Content in blood[b] (mg/mL)	Added (mg/mL)	Found (mg/mL)	RSD (%, $n=3$)	Recovery (%)
1	0.058	116	0.1	0.151	1.9	93.31
2	0.066	132	0.1	0.165	1.5	99.82
3	0.074	148	0.1	0.175	1.2	101.24

[a]The Hb content in the blood of healthy women and men is 120–160 and 130–180 mg/mL, respectively [35]

[b]The content of Hb in the blood samples before dilution

degree of WS_2 QDs was not obviously changed, with the existence of Glu, BSA, HIgG, Cl^-, K^+, Na^+, and Ca^{2+} in the system (relative error less than ±5%, Fig. 5). Therefore, this method exhibited selective detection of Hb and Myo, which can be expected to be applied for clinical detection.

Analysis of Hb and Myo in human blood samples

To evaluate the practicality of the method, it was used to determine the Hb content in the blood of two healthy women and one healthy man under fasting conditions. See the Experimental section for the pretreatment of blood samples. The experimental results are shown in Table 2. The Hb levels in the blood of the two women were 116 and 132 mg/mL, respectively. The Hb level in the blood of the man was 148 mg/mL. All levels were in line with the normal range [35]. To explore the reliability of the experimental method, recovery experiments were carried out. The results were 93.31–101.24%, and the corresponding RSD were 1.2–1.9%, all of which were less than 2.0%, showing good precision.

In addition, this method was also applied to determine Myo content in the serum of three healthy people under fasting conditions. As serum samples of healthy people contain very little Myo, a certain amount of Myo standard was added to the serum sample to simulate patient serum. After tenfold dilution with PBS 7.5, the experiments were carried out, and results are shown in Table 3. The recoveries were 95.01–97.00%. Therefore, WS_2 QDs have potential use as sensors for the efficient detection of Hb/Myo in real blood samples.

Table 3 Detection results of Myo in human serum samples [a]

Samples	Measured value (μg/mL)	Added (μg/mL)	Found (μg/mL)	RSD (%, $n=3$)	Recovery (%)
1	ND[b]	0.020	0.019	1.8	95.01
2	ND	0.050	0.048	1.5	96.24
3	ND	0.100	0.097	1.2	97.00

[a]Diagnostic limit of Myo in serum: >0.1 μg/mL [3]

[b]Not detected

Conclusion

In summary, WS_2 QDs with high QY (11.23%) were synthesized using $Na_2WO_4{\cdot}2H_2O$ and GSH under simple one-step hydrothermal conditions and exhibited great photo-bleaching resistance, salt tolerance, and pH stability. The obtained WS_2 QDs are the first example of TMD QDs without any modification as a highly sensitive and selective fluorescent sensor for simultaneous Hb and Myo detection, with detection limits as low as 260 and 7.6 ng/mL, respectively. Importantly, WS_2 QDs were used to determine Hb/Myo content in human blood/serum samples, with satisfactory results. Therefore, this technique holds promise for the development of new methods for actual diagnostic and biochemical analysis of Hb and Myo.

Supplementary Information The online version contains supplementary material available at https://doi.org/10.1007/s00216-021-03784-9.

Acknowledgments The authors appreciate financial support from the Education Department Science Foundation of Liaoning Province, China (LJ2020010) and the PhD Research Start-up Foundation of Liaoning Normal University, China (BS2020L008, 203070091905).

Declarations

Conflict of interest The authors declare that they have no competing interests.

Ethical approval The study was approved by the Ethics Committee of Liaoning Normal University (LL2021030) and was performed in accordance with the ethical standards. All blood samples were taken from healthy volunteers in our lab.

Consent to participate All samples were taken after obtaining signed consent from the volunteers.

References

1. Zhou TC, Ashley J, Feng XT, Sun Y. Detection of hemoglobin using hybrid molecularly imprinted polymers/carbon quantum dots-based nanobiosensor prepared from surfactant-free Pickering emulsion. Talanta. 2018;190:443–9.

2. Yj Z, Yj C, Fang MY, Tian YB, Bai GY, Zhuo KL. Silanized carbon dot-based thermo-sensitive molecularly imprinted fluorescent sensor for bovine hemoglobin detection. Anal Bioanal Chem. 2020;412:5811–7.
3. Miao DW, Liu DK, Zeng YB, Zhou GB, Xie W, Yang YW, et al. Fluorescent aptasensor based on D-AMA/F-CSC for the sensitive and specific recognition of myoglobin. Spectrochim Acta A. 2020;228:117714.
4. Sullivan MV, Stockburn WJ, Hawes PC, Mercer T, Reddy SM. Green synthesis as a simple and rapid route to protein modified magnetic nanoparticles for use in the development of a fluorometric molecularly imprinted polymer-based assay for detection of myoglobin. Nanotechnology. 2021;32:095502.
5. Mandani S, Rezaei B, Ensafi AA, Rezaei P. Ultrasensitive electrochemical molecularly imprinted sensor based on AuE/Ag-MOF@MC for determination of hemoglobin using response surface methodology. Anal Bioanal Chem. 2021;413:4895–906.
6. Deng Y, Wen ZR, Cheng H, Yan LJ, Shao B, Li GJ, et al. SnO_2 quantum dots functionalized 3D graphene composite for enhanced performance of electrochemical myoglobin biosensor. Int J Electrochem Sci. 2020;15:10412–22.
7. Swaminathan N, Nerthigan Y, Wu HF. Polyaniline stabilized silver (I) oxide nanocubes for sensitive and selective detection of hemoglobin in urine for hematuria evaluation. Microchem J. 2020;155:104723.
8. Liu YH, Wang YH, Jiang K, Sun S, Qian SH, Wu QP. A persistent luminescence-based label-free probe for the ultrasensitive detection of hemoglobin in human serum. Talanta. 2020;206:120206.
9. Shorie M, Kumar V, Sabherwal P. Carbon quantum dots-mediated direct fluorescence assay for the detection of cardiac marker myoglobin. Curr Sci. 2015;108:1595–6.
10. Moreno Y, Song QG, Xing ZK, Sun YZ, Yan ZJ. Hybrid tilted fiber gratings-based surface plasmon resonance sensor and its application for hemoglobin detection. Chin Opt Lett. 2020;18:100601.
11. Murahashi M, Makinodan M, Yui M, Hibi T, Kobayashi M. Immunochromatographic detection of human hemoglobin from deteriorated bloodstains due to methamphetamine contamination, aging, and heating. Anal Bioanal Chem. 2020;412:5799–809.
12. Van Bommel MR, De Jong APJM, Tjaden UR, Irth H, Van der Greef J. High-performance liquid chromatography coupled to enzyme-amplified biochemical detection for the analysis of hemoglobin after pre-column biotinylation. J Chromatogr A. 2000;886:19–29.
13. Kalaiyarasan G, Joseph J. Cholesterol derived carbon quantum dots as fluorescence probe for the specific detection of hemoglobin in diluted human blood samples. Mater Sci Eng C. 2019;94:580–6.
14. Guo YN, Park T, Yi JW, Henzie J, Kim J, Wang ZL, et al. Nanoarchitectonics for transition-metal-sulfide-based electrocatalysts for water splitting. Adv Mater. 2019;31:1807134.
15. Sun J, Wang Y, Guo S, Wan B, Dong L, Gu Y, et al. Lateral 2D WSe_2 p-n homojunction formed by efficient charge-carrier-type modulation for high-performance optoelectronics. Adv Mater. 2020;32:1906499.
16. Kim J, Lee Y, Kang M, Hu L, Zhao SF, Ahn JH. 2D materials for skin-mountable electronic devices. Adv Mater. 2021;2005858.
17. Singh VK, Mishra H, Ali R, Umrao S, Srivastava R, Abraham S, et al. In situ functionalized fluorescent WS_2-QDs as sensitive and selective probe for Fe^{3+} and a detailed study of its fluorescence quenching. ACS Appl Nano Mater. 2019;2:566–76.
18. Suh JM, Kwon KC, Lee TH, Kim C, Lee CW, Song YG, et al. Edge-exposed WS_2 on 1D nanostructures for highly selective NO_2 sensor at room temperature. Sensors Actuators B-Chem. 2021;333:129566.
19. Jiang DL, Sheng KK, Gui GY, Jiang H, Liu XM, Wang LF. A novel smartphone-based electrochemical cell sensor for evaluating the toxicity of heavy metal ions Cd^{2+}, Hg^{2+}, and Pb^{2+} in rice. Anal Bioanal Chem. 2021;413:4277–87.
20. Chen CJ, Yeh CY, Chen CH, Jena A, Wei DH, Chang H, et al. Molybdenum tungsten disulfide with a large number of sulfur vacancies and electronic unoccupied states on silicon micropillars for solar hydrogen evolution. ACS Appl Mater Interfaces. 2020;12:54671–82.
21. Rao TK, Wang HD, Zeng YJ, Guo ZN, Zhang H, Liao WG. Phase transitions and water splitting applications of 2D transition metal dichalcogenides and metal phosphorous trichalcogenides. Adv Sci. 2021;8:2002284.
22. Yadav V, Roy S, Singh P, Khan Z, Jaiswal A. 2D MoS_2-based nanomaterials for therapeutic, bioimaging, and biosensing applications. Small. 2019;15:1803706.
23. Meng S, Zhang YY, Wang HD, Wang LD, Kong TT, Zhang H, et al. Recent advances on TMDCs for medical diagnosis. Biomaterials. 2021;269:120471.
24. Zhao X, He DW, Wang YS, Fu C. Facile fabrication of tungsten disulfide quantum dots (WS_2 QD) effective probes for fluorescence detection of dopamine (DA). Mater Chem Phys. 2018;207:130–4.
25. Yin WX, Liu X, Zhang XY, Gao XP, Colvin VL, Zhang YY, et al. Synthesis of tungsten disulfide and molybdenum disulfide quantum dots and their applications. Chem Mater. 2020;32:4409–24.
26. Guo XR, Wang Y, Wu FY, Ni YN, Kokot S. The use of tungsten disulfide dots as highly selective, fluorescent probes for analysis of nitrofurazone. Talanta. 2015;144:1036–43.
27. Yan YH, Zhang CL, Gu W, Ding CP, Li XC, Xian YZ. Facile synthesis of water-soluble WS_2 quantum dots for turn-on fluorescent measurement of lipoic acid. J Phys Chem C. 2016;120:12170–7.
28. Hang DR, Sun DY, Chen CH, Wu HF, Chou MMC, Islaml SE, et al. Facile bottom-up preparation of WS_2-based water-soluble quantum dots as luminescent probes for hydrogen peroxide and glucose. Nanoscale Res Lett. 2019;14:271.
29. Mani NP, Cyriac J. Hydrothermal synthesis of WS_2 quantum dots and their application as a fluorescence sensor for the selective detection of 2,4,6-trinitrophenol. New J Chem. 2020;44:10840–8.
30. Kim MJ, Jeon SJ, Kang TW, Ju JM, Yim DB, Kim HI, et al. 2H-WS_2 quantum dots produced by modulating the dimension and phase of 1T-nanosheets for antibody-free optical sensing of neurotransmitters. ACS Appl Mater Interfaces. 2017;9:12316–23.
31. Yan FY, Sun ZH, Xu JX, Li HJ, Zhang YY. WS_2 quantum dots-MnO_2 nanosheet system for use in ratiometric fluorometric/scattered light detection of glutathione. Microchim Acta. 2020;187:344.
32. Yi ZH, Li XM, Zhang HY, Ji XL, Sun W, Yu YX, et al. High quantum yield photoluminescent N-doped carbon dots for switch sensing and imaging. Talanta. 2021;222:121663.
33. Zhang SY, Wang Y, Yang G. A facile strategy for the preparation of carboxymethylcellulose-derived polymer dots and their application to detect tetracyclines. Macromol Chem Phys. 2021;222:2100267.
34. Wang HY, Lu QJ, Hou YX, Liu YL, Zhang YY. High fluorescence S, N co-doped carbon dots as an ultra-sensitive fluorescent probe for the determination of uric acid. Talanta. 2016;155:62–9.
35. Barati A, Shamsipur M, Abdollahi H. Hemoglobin detection using carbon dots as a fluorescence probe. Biosens Bioelectron. 2015;71:470–5.